Journal of Zhejiang University-SCIENCE A (Applied Physics & Engineering)
ISSN 1673-565X (Print); ISSN 1862-1775 (Online)
www.jzus.zju.edu.cn; www.springerlink.com
E-mail: jzus@zju.edu.cn

Test technology research and fatigue damage prediction of a car body based on dynamic simulation load spectrum*

Lu JIA, Huan-yun DAI, Ye SONG†‡

State Key Laboratory of Traction Power, Southwest Jiaotong University, Chengdu 610031, China

†E-mail: sy8621@163.com

Received Dec. 25, 2019; Revision accepted Apr. 10, 2020; Crosschecked Oct. 16, 2020

Abstract: The dynamic model of a high-speed electric multiple unit (EMU) is established based on the theory of rigid-flexible coupling multi-body system dynamics. Depending on the actual operating conditions of the vehicle, there are a variety of conditions of car body load-time history. We assess ineffective amplitude omission, load spectrum extrapolation, and extreme determination through the car body load-time history, and then obtain the car body fatigue load block spectrum. Finally, we perform a fatigue strength test on the whole car body on a car body fatigue test bench. It is shown that the accelerations of the three directions of the vehicle car body increase with increasing speed. When the train passes a curve, the lateral acceleration average becomes greater. There is also an increase in the car body accelerations in three directions when the train goes through a turnout or twisted line. Under the condition of a failed spring, the vertical acceleration of the car body is obviously increased. Anti-yaw damper failure will cause a significant increase in vehicle lateral acceleration. The failure of lateral and vertical dampers on the second suspension causes an insignificant acceleration increase in three directions. The car body acceleration increases the wear-type profile relative to the original profile in various working and speed level conditions a little. The influence on the damage of vehicle car body under various working conditions is predicted according to the obtained load spectrum.

Key words: Dynamic model; Car body; Load-time history; Fatigue; Damage
https://doi.org/10.1631/jzus.A1900662 **CLC number:** U270.1

1 Introduction

The car body is subjected to complex alternating loads during normal operation, and its failure form is a typical fatigue failure. In recent years, with the increase of train running speeds, the load on the car body has become increasingly complicated, the use conditions have become more severe, and the probability of fatigue damage is increasing (Gou et al., 2015; Yang et al., 2017). Domestic and foreign scholars have carried out many studies on the fatigue strength of the car body, which are summarized as follows.

Gutiérrez-Carvajal et al. (2018) carried out experimental research on a full-size car body chassis to support car body design. Jun et al. (2010) in Korea evaluated the cracks in the electric multiple unit (EMU) chassis. Gongjiang (2003) in Japan systematically analyzed the load acting on the vehicle body and obtained effective conclusions. Zhang (2008) proposed the use of the stress-number (S-N) curves of steel and aluminum alloy materials to predict the life of a car body. Much research work has been carried out on the strength test. Researchers from Korea Railroad Research Institute (KRRI) conducted a simulated fatigue test in a laboratory using a full-size stainless steel body as the research object (Oomura et al., 1992).

‡ Corresponding author
* Project supported by the Science and Technology Innovation Program of Central Universities (No. 2682019CX45), China
ORCID: Lu JIA, https://orcid.org/0000-0001-5339-7433

In China, Xue (2013) analyzed measured data of load-time history. He proposed a combination of Weibull distribution and log-normal distribution for describing the load spectrum distribution law of rail vehicles and verified its effectiveness through distribution verification. Zhang (2016) used the quasi-static superposition method to analyze the fatigue damage of a car body under random load and compared it with the fatigue damage calculated by accelerated load block spectrum. Hou (2016) appropriately extrapolated the car body acceleration load-time history measured in the line test and compiled the measured load spectrum of a car body running 1.5×10^7 km before and after the Wheelset-class-lathing. Qin (2017) used the CRH0503 intermediate car body of the Chinese standard EMU as the research object, combined with an actual measurement and simulation calculation, and studied the load transfer relationship. According to the starting conditions in the actual line, high-speed tunnel crossing, low-speed crossing turnout, and other line conditions, the load characteristics of each load system on the car body were analyzed. Based on comprehensive consideration of the effects of stress corrosion on aluminum alloys, Wang (2015) applied fatigue strength and fracture mechanics theory to analyzing the crack initiation life and crack propagation life of the welds in the key parts of the car body pillow beam. Based on the principles of vibration mechanics and fatigue analysis, Wang (2016) performed vibration fatigue analysis on the body of straddle-type monorail vehicles and compared the stress spectrum data measured using quasi-static methods and tests. Li (2018) researched a calculation method of vibration fatigue dynamic stress suitable for the body of an EMU, so as to obtain the time history of the vibration fatigue dynamic stress of the vehicle body structure under multiple load input conditions and to evaluate the vibration intensity of the vehicle body based on the stress simulation results. Liu (2015) comparatively analyzed the applicability of different numerical simulation methods in the train flow calculation, compiled the aerodynamic load spectrum of the equipment cabin, and performed a fatigue damage analysis of the skirting board. Wei (2018) carried out research on fatigue crack propagation behaviors on the A7N01-T5 aluminum alloy bottom beams commonly used in high-speed EMU trains. Lu et al. (2018a, 2018b) used a decoupling method to study the influence mechanism of vibration, aerodynamic load, welding residual stress, and other static random variables on vehicle body fatigue under high-speed conditions, and used the method of coupling various factors to study the prediction of vehicle body fatigue life. Song et al. (2016) used the vehicle body fatigue test rig built by Southwest Jiaotong University, China to determine the extreme value of the load block spectrum with the mean and amplitude distribution functions of the load spectrum, and generated a standard load block spectrum for fatigue tests. The vehicle body fatigue test method includes the vehicle body constant amplitude loading test, variable amplitude block spectrum loading test, random load test, and vehicle aerodynamic load fatigue test. The dynamic stress of key parts of the vehicle body was tested and car body fatigue life was evaluated. Miao et al. (2010) studied the typical fatigue load spectrum extrapolation algorithm of a rail vehicle structure by combining multi-body dynamics and finite element simulation. Yan (2009) carried out research on the longitudinal load of heavy-duty trains on the Da-Qin line. In that study, the scheme of longitudinal load test was proposed. Yan (2014) reversed the equivalent load spectrum according to the load transfer coefficient obtained from the calibration of the indoor equipment cabin floor. Liu (2013) evaluated the fatigue strength of CRH3 based on the nominal stress IIW (International Institute of Welding) standard and then used the standard of American Society of Mechanical Engineers (ASME) to evaluate the fatigue of the car body with the equivalent structural stress. Ju (2013) predicted the fatigue life of the aluminum alloy car body weld of a high-speed EMU. Lu (2010) used the Craig-Bampton fixed interface modal synthesis method to simultaneously simulate the load spectrum of the CRH5 car body with the kinetic software ADAMS and evaluate the fatigue life of the car body. Li (2008) proposed a fatigue life prediction method for railway vehicle weld structures based on a virtual fatigue test on the basic theory and method of fatigue life prediction of such structures. A model establishment method and the selection principle of fatigue evaluation point in finite element simulation were established. The advantages and disadvantages of the

three standards (AAR, 1999; BSI, 2014; IIW, 2016) for structural fatigue life prediction were compared.

In summary, how to accurately obtain the vehicle body load spectrum becomes a key factor for predicting and determining the fatigue damage of the vehicle body. The vehicle body load spectrum is also the processing result of the load-time history of the train body, which can reflect the vehicle body load. The size and distribution law are the basis for evaluating the fatigue strength of the car body.

In this study, the dynamic model is used to simulate various line conditions, various speed levels, various fault conditions, and different treads, and the acceleration load spectrum of the vehicle body is obtained. The life spectrum prediction analysis of the vehicle body structure is carried out using the obtained load spectrum. By processing the obtained load spectrum, the fatigue load spectrum of the vehicle body that can be used for the bench test is compiled, and finally applied on the test bench.

2 Rigid-flexible coupling multi-body system dynamics modeling

Multi-body system dynamics simulation is used to study the relationship between displacement, velocity, acceleration, angular velocity, moment, and force of various rigid bodies or flexible parts inside the system (Yang, 2005; Xie et al., 2010). In order to study the vehicle body load spectrum more accurately, SIMPACK software is used to establish the rigid-flexible multi-body dynamics model of the train. In the model, the car body is considered as a flexible body, and other parts are processed as rigid bodies. The process of establishing the elastomer model in SIMPACK is shown in Fig. 1.

In the finite element method, the establishment of the elastic body needs to reduce the degree of freedom (generally to not more than 10000). In this study, the finite element analysis software ANSYS uses the Guyan reduction method to reduce the car body model. The reduction of the degree of freedom needs to consider the accuracy of the model. The Guyan method effectively reduces the body mass matrix and the stiffness matrix to each degree of freedom in the calculation of the natural frequency and formation. The final rigid-flexible coupling dynamics model is shown in Fig. 2.

3 Dynamics simulation case settings

The train running line can be basically divided into four line conditions: straight line segment, curved section, train passing track, and twisted line. According to the wheel-rail relationship of the vehicle, it can be divided into non-wearing type tread surfaces and wear type tread surfaces. According to the state of the vehicle, it can be divided into normal state and fault condition. The fault condition includes the failure of the air spring, the failure of the lateral damper,

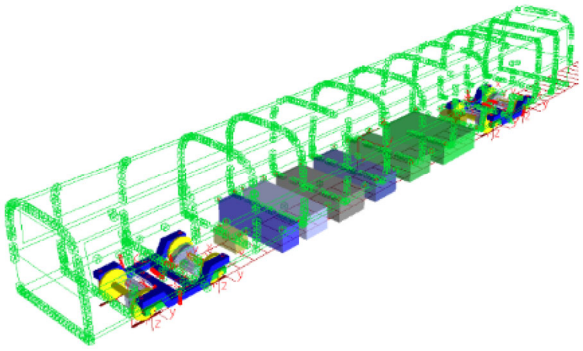

Fig. 2 Rigid-flexible coupling dynamics model

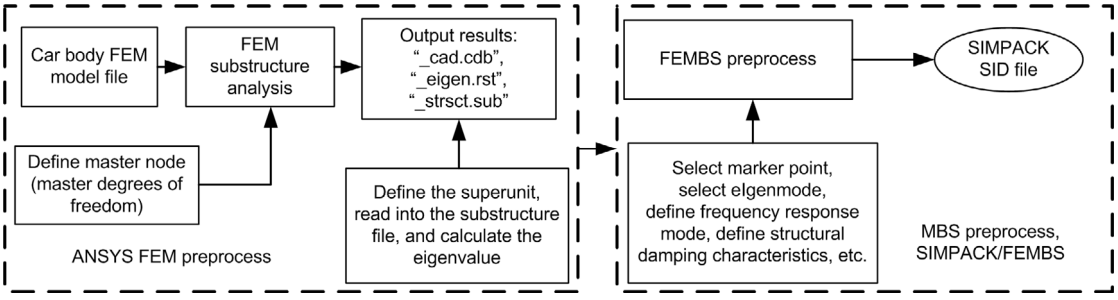

Fig. 1 Process of generating SID by using finite element model builder

FEM: finite element method; SID: system identification data; FEMBS: finite element multi-body system; MBS: multi-body system

and the failure of the anti-yaw damper. Considering the vehicle status and line conditions, the simulation conditions listed in Table 1 are designed to obtain the vehicle body acceleration load spectrum. Different speed levels for straight lines, curves, turns, and twisted lines are considered in the operating conditions. In the curve section, the radius is 7000 m and the super-high is 130 mm; the turnout uses the No. 58 ballast; the twisted line curve radius is 300 m. Factors such as air spring failure and damper failure at different speed levels are considered in the fault conditions. At the same time, traction braking conditions are considered during the running on the straight section. The calculation of all working conditions is divided into two types: non-abrasive tread (S1002CN) and wear tread (S1002CNwg2).

Table 1 Dynamic simulation cases

Trial	Case/Condition	Speed rating (km/h)
Normal case	1 (straight line)	100–400
	2 (curve)	100–350
	3 (turnout)	100–220
	4 (twist)	20–50
	5 (traction)	100–350
Fault case	6 (air spring failure)	100–350
	7 (secondary vertical damper failure)	100–350
	8 (lateral damper failure)	100–250
	9 (anti-hunting damper failure)	100–250

4 Simulation load spectrum analysis

According to the established dynamic model, the dynamic simulation of the cases in Table 1 is carried out to obtain the vibration acceleration load spectrum of the vehicle body. The load spectrum is a random spectrum of time series. In order to understand the information in the load spectrum more intuitively, it is statistically analyzed to obtain its amplitude and frequency.

The energy of a random signal may be difficult to observe in the time domain, but it is often clear in the frequency domain. The vibration process of a random signal can be expressed in the frequency domain by a power spectral density (PSD) function in addition to the representation of the variance, the mean, and the correlation function in the time domain. The PSD function is defined as the mean square value of the spectral density, which represents the distribution of the vibrational energy of the random signal over frequency. Therefore, the PSD function is defined as

$$W_x(f)=\frac{1}{\Delta f}\left[\lim_{T\to\infty} x_{\Delta f}^2(t)\mathrm{d}t\right], \tag{1}$$

which represents the ratio of the mean squared value to the bandwidth of the random variable $x_{\Delta f}$ in the bandwidth Δf. In Eq. (1), T is the cumulative time, and t is the unit time. In general, PSD represents the average power spectrum distribution of the signal over the frequency range and represents the frequency response of the structure to random vibration loads; it is ultimately expressed as a correlation curve of PSD and frequency.

4.1 Acceleration analysis of the vehicle center at different speeds

The different speeds of the nine operating conditions in Table 1 were simulated to obtain the load spectrum of the vehicle center acceleration. Fig. 3 shows the load-time history diagram of the vehicle center acceleration under normal running conditions of the vehicle body at 400 km/h and 350 km/h. From the figure and simulation analysis results, at 400 km/h the vertical acceleration amplitude is within 0.08g (g is the acceleration of gravity), the lateral acceleration amplitude is within 0.11g, and the longitudinal acceleration amplitude is within 0.06g. At 350 km/h, the vertical acceleration amplitude is within 0.06g, the lateral acceleration amplitude is within 0.08g, and the longitudinal acceleration amplitude is within 0.05g. The vehicle body center acceleration increases with the increase of running speed under various working conditions. Except for working condition 5, with the increase of running speed the acceleration of the car body is greater in the lateral and vertical directions.

Figs. 4–6 show the rain flow count histogram of the center acceleration of the car body in three directions under normal conditions at 350 km/h and 400 km/h. It can be seen from the figures that, as the running speed increases, the amplitudes of the vertical and lateral vibrations of the car body increase significantly, but not that in the longitudinal direction. It

can be seen from the PSD diagram of the vehicle body acceleration in Fig. 7 that the vibration energy of the vehicle body is mainly concentrated below 20 Hz, and the vibration of the vehicle body is a low-frequency vibration process.

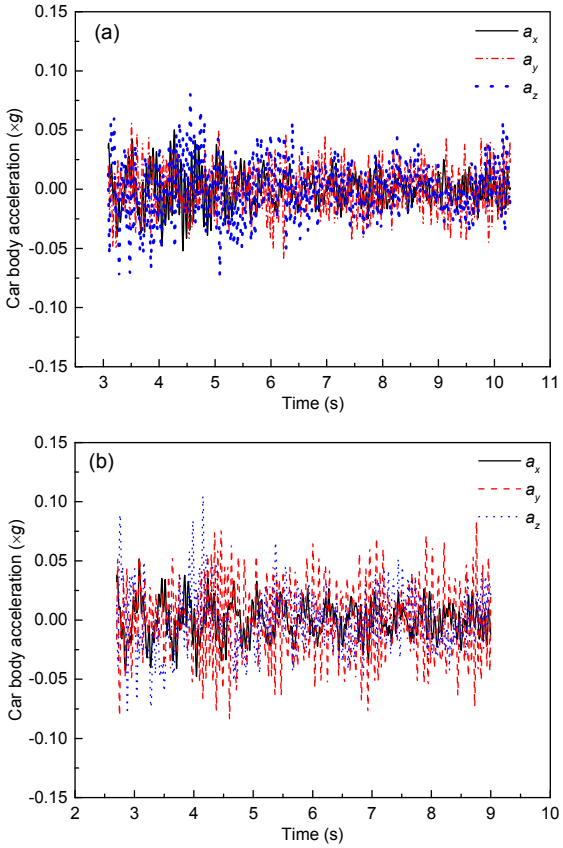

Fig. 3 Car body vibration accelerations in a straight line: (a) 350 km/h; (b) 400 km/h (a_x, a_y, and a_z are the longitudinal, lateral, and vertical accelerations of vehicle body, respectively)

4.2 Acceleration analysis of vehicle body under different line conditions

Comparing and analyzing the simulation results of working conditions 1–4 in Table 1, it can be observed that when the vehicle body runs in the straight line segment at 300 km/h, the vertical acceleration amplitude is within 0.06*g*, the lateral acceleration amplitude is within 0.05*g*, the longitudinal acceleration amplitude is within 0.04*g*, and the acceleration average in all directions is basically zero. On 300-km/h curve segment runs, the vertical acceleration amplitude is within 0.05*g*, the lateral acceleration amplitude is within 0.06*g*, the longitudinal

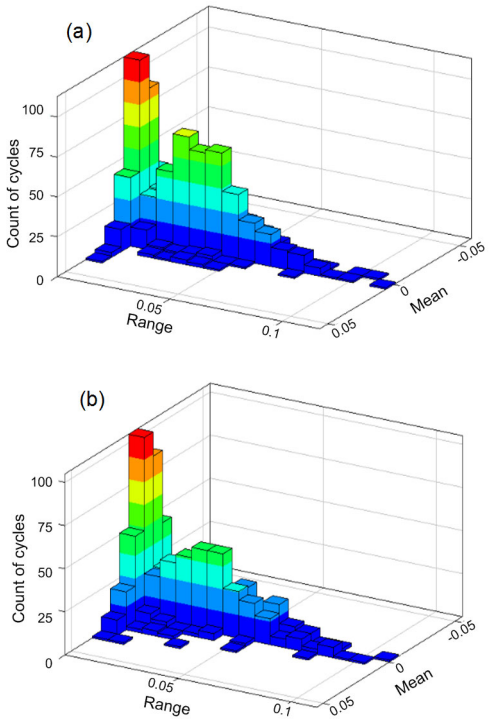

Fig. 4 Rain flow histograms for a_x of 350-km/h (a) and 400-km/h (b) car body in a straight line

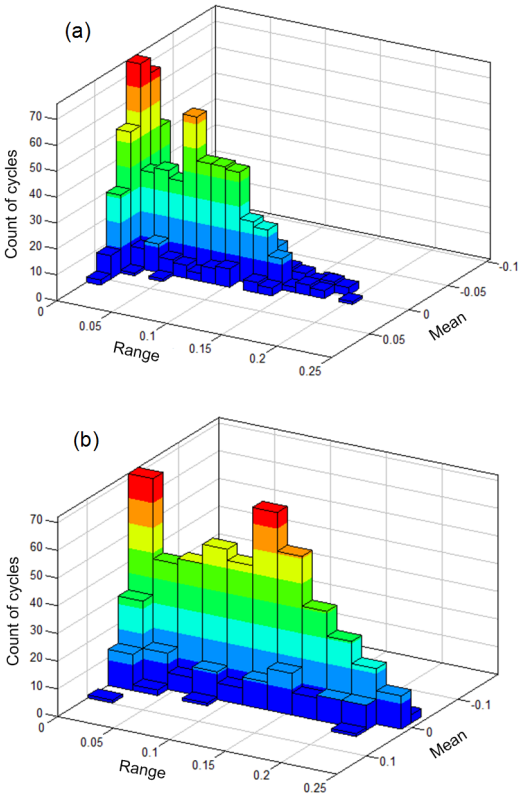

Fig. 5 Rain flow histograms for a_y of 350-km/h (a) and 400-km/h (b) car body in a straight line

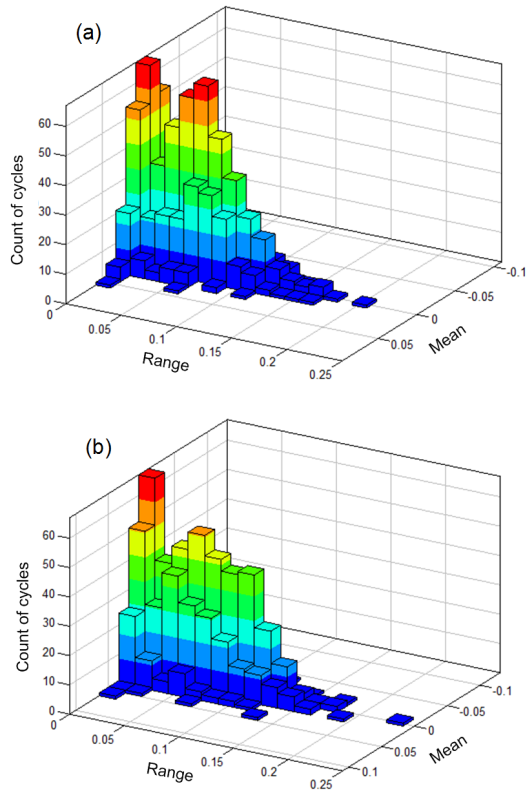

Fig. 6 Rain flow histograms for a_z of 350-km/h (a) and 400-km/h (b) car body in a straight line

acceleration amplitude is within 0.04*g*, the lateral acceleration average is large; when passing the ballast at 220 km/h, the vertical acceleration amplitude is within 0.10*g*, the lateral acceleration amplitude is within 0.12*g*, and the longitudinal acceleration amplitude is within 0.07*g*. The average value of the vertical and lateral accelerations is significantly higher than that of the straight line. When passing over twisted line at 50 km/h, the acceleration amplitude is small due to the low speed. The vertical acceleration amplitude is within 0.015*g*, the lateral acceleration amplitude is within 0.030*g*, the longitudinal acceleration amplitude is within 0.006*g*, and the mean vertical and lateral accelerations fluctuate significantly.

After the rain flow treatment, it is found that the lateral acceleration amplitude and the mean value increase significantly when running in a curved section. Over ballast, the vertical and lateral acceleration amplitudes of the vehicle body also change significantly. For the twisted line, because of the low speed, the amplitude of the vibration is small. Through the PSD analysis of the vehicle body acceleration, it can be seen that the vibration energy of the vehicle body is mainly concentrated below 20 Hz when travelling on a straight line, on a curve or over ballast. On the twisted path, the vibration energy of the vehicle body is mainly concentrated below 10 Hz.

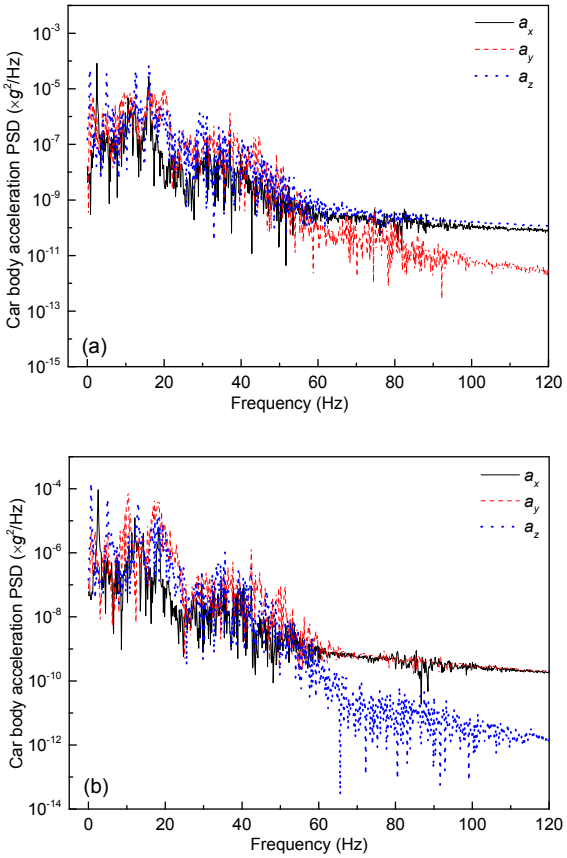

Fig. 7 PSD for 350-km/h (a) and 400-km/h (b) car body acceleration in a straight line

4.3 Acceleration analysis of vehicle body under fault conditions

Comparing and analyzing the simulation results of working conditions 6–9 in Table 1, it can be seen that the vertical acceleration amplitude of the car body increases significantly when an air spring fails, reaching 0.15*g*, the lateral acceleration amplitude is within 0.08*g*, the longitudinal acceleration amplitude reaches 0.04*g*, and the acceleration average in all directions is basically zero. When the anti-yaw damper fails, the vertical acceleration amplitude is 0.04*g*, the lateral acceleration amplitude increases

significantly, reaching 0.17*g*, and the longitudinal acceleration amplitude reaches 0.03*g*. When the secondary lateral damper fails, the vertical acceleration amplitude is within 0.05*g*, the lateral acceleration amplitude is within 0.05*g*, and the longitudinal acceleration amplitude reaches 0.05*g*. When the secondary vertical damper fails, the vertical acceleration amplitude is within 0.05*g*, the lateral acceleration amplitude is within 0.05*g*, and the longitudinal acceleration amplitude is within 0.05*g*. It can be seen that the air spring and the anti-yaw damper have good stabilizing effects on the vertical and lateral vibrations of the vehicle body, respectively. When either fails, the corresponding vehicle body acceleration amplitude has a significant increase. The failure of the secondary vertical and lateral dampers has a certain influence on the accelerations of the three directions of the car body, but it is less compared with that following from failure of the air spring or the anti-yaw damper.

After the rain flow treatment, it is found that the vertical acceleration amplitude increases significantly when the air spring fails; when the anti-yaw damper fails, the lateral acceleration amplitude of the vehicle body increases significantly, and when the secondary vertical and lateral dampers fail, the acceleration amplitudes in all three directions increase noticeably. Through PSD analysis of the vehicle body, it can be seen that when the anti-yaw damper fails, the vibration energy of the secondary lateral and vertical dampers is mainly concentrated below 10 Hz. When the air spring fails, the vibration energy of the car body is mainly concentrated below 30 Hz.

4.4 Acceleration analysis of different wheel treads

When the EMU has reached a certain mileage, the wheel tread will have a certain degree of wear, and it is necessary to repair the tread. Generally, the tread near the repair is called the tread after wear. Fig. 8 shows the load-time history of the vehicle body acceleration during running at 300 km/h over the straight line segment and the curved section under the condition of the tread after wear. From the results of simulation analysis, it can be seen that when the vehicle body runs in a straight line at 300 km/h, the vertical acceleration amplitude is within 0.07*g*, the lateral acceleration amplitude is within 0.08*g*, and the longitudinal acceleration amplitude is within 0.05*g*. For a curve at 300 km/ h, the vertical acceleration amplitude is within 0.08*g*, the lateral acceleration amplitude is within 0.08*g*, and the longitudinal acceleration amplitude is within 0.04*g*. The lateral acceleration average is large whether it is straight line, curve, or turnout or twisted line. After wear, the accelerations of the car body in three directions are higher than those with the original tread, and the acceleration amplitude of the car body increases with speed.

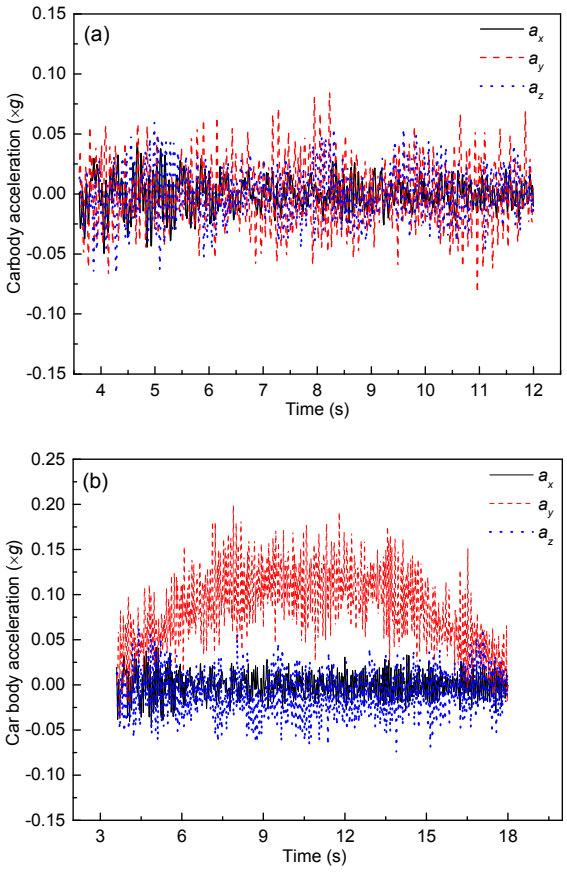

Fig. 8 300-km/h car body vibration acceleration in straight line (a) and curve (b)

After the rain flow treatment, it is found that the lateral acceleration amplitude and the mean value of the vehicle body increase significantly on a curve segment. Compared with the straight running result, the acceleration amplitudes of the three directions of the car body show a significant increase. Through PSD analysis of the vehicle body acceleration, it can be shown that the vibration energy of the vehicle body is mainly concentrated below 20 Hz.

5 Fatigue-life assessment of car body structure

In this study, the stress-life prediction method is used to predict the life of the vehicle body structure. The technical route adopted is shown in Fig. 9.

In fatigue-life prediction analysis, some scatter points and certain levels of stress amplitude are often included, so the fatigue life is assumed to obey a lognormal distribution. Gauss defines the probability density function of a variable x as

$$\phi(x)=\frac{1}{\sigma\sqrt{2\pi}}\mathrm{e}^{\frac{(x-\varphi)^2}{2\sigma^2}}, \tag{2}$$

and so the cumulative probability of the variable x is expressed as

$$\Phi(x)=\frac{1}{2}\left(1+\mathrm{erf}\frac{x-\varphi}{\sigma\sqrt{2}}\right). \tag{3}$$

In the fatigue analysis, x=lg$N$, φ=lgN_{50}, N represents the fatigue life under load cycle conditions, N_{50} represents the number of cycles in which 50% of the test specimens predict failure, and σ represents the standard deviation corresponding to the S-N curve of lg$N$.

The stress-life curve is then obtained:

$$N=\frac{A}{S-E_{\mathrm{B}}}\exp\left[-\left(\frac{S-E_{\mathrm{B}}}{B}\right)^{C}\right], \tag{4}$$

where A, B, C and E_{B} are determined by the material itself. S is the stress; A is called the Bastenaire coefficient and represents the parameter point on the life curve; B represents the scale factor; C represents the Bastenaire index; E_{B} represents the Bastenaire fatigue limit. When C>1, the S-N curve has an inflection point. When C=0, the model is simplified to

$$N=\frac{A}{\mathrm{e}(S-E_{\mathrm{B}})}. \tag{5}$$

Correcting the Bastenaire curve to the discrete factor and normal distribution law, we have

$$N_{p\%}=\frac{A}{S\pm\sigma_{\mathrm{m}}\sigma_{\mathrm{s}}-E_{\mathrm{B}}}\exp\left[-\left(\frac{S\pm\sigma_{\mathrm{m}}\sigma_{\mathrm{s}}-E_{\mathrm{B}}}{B}\right)^{C}\right], \tag{6}$$

where $N_{p\%}$ is the fatigue life modified by the Bastenaire curve, the discrete factor σ_{s} represents the standard deviation of stress, and σ_{m} represents the standard deviation associated with the mean.

Ultimately, linear damage is expressed as 1/N. According to the simulation of the vehicle body load spectrum and the finite element analysis results under the unit load condition obtained by the finite element, the fatigue life analysis is performed in nCode software, and the car body base material and the weld bead are grouped in the life analysis. Considering the different material properties, the correction of the S-N curve takes into account material factors such as material thickness, roughness, residual stress, and

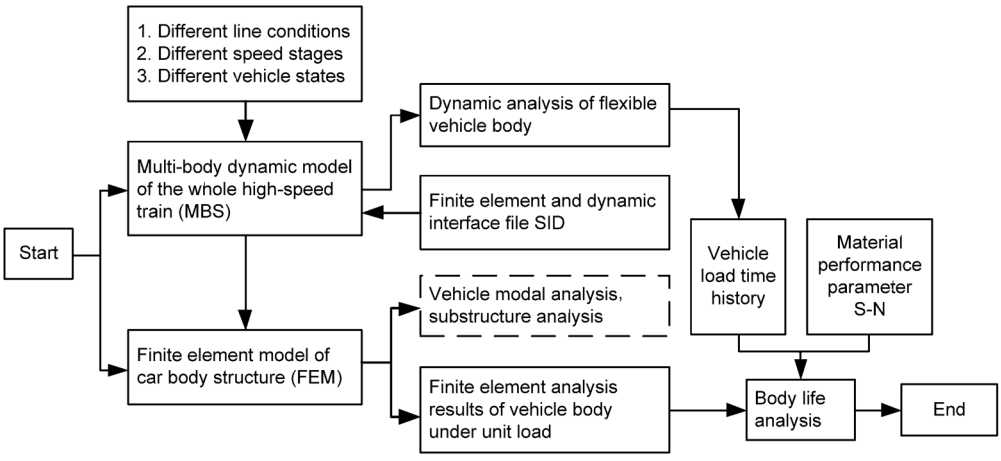

Fig. 9 Technology roadmap of life prediction for car body

average stress. For the correction of the average stress, the Forschungskuratorium Maschinenbau (FKM) average stress correction method is adopted. Finally, the damage list under the speed level corresponding to each working condition in Tables 2 and 3 is obtained.

The speed levels V1–V7 in the tables respectively correspond to the speeds of the various working conditions in Table 1. Since the line lengths in each working condition or the single-pass ballast have small effect on the vehicle body, they are rounded up. It can be seen from the two lists that the damage value is less than 1, indicating that the vehicle body has not reached a state of damage under the condition of the rectification.

Fig. 10a shows the damage values per 10000 km at various speed levels of the car body under the conditions of two tread forms, with the linear operating condition, the air spring failure, the failure of the secondary vertical damper, the failure of the lateral damper, and the failure of the anti-yaw damper. It can be seen from the figure that, under the same conditions, the tread after abrasion is more damaged than the non-abrasive tread, and the damage is also increased with increased speed; when the speed is low, the damage is very small except for the failure condition of the air spring, basically close to the normal straight running condition; from the vertical comparison in the figure, when the vehicle speed is below 200 km/h (V3), the air spring failure has the greatest damage to the car body. When the speed is higher than 200 km/h, the anti-yaw failure has the greatest damage to the car body. The failure of the device has the greatest influence on the damage value of the vehicle body; the effect on the damage of the vehicle body of a lateral damper failure is less than that of a vertical damper failure.

Table 2 List of damage under new-tread cases

Trial	Case	Damage							Remark
		V1 (100 km/h)	V2 (150 km/h)	V3 (200 km/h)	V4 (250 km/h)	V5 (300 km/h)	V6 (350 km/h)	V7 (400 km/h)	
Normal case	1	6.9×10^{-7}	5.9×10^{-6}	8.0×10^{-6}	6.7×10^{-6}	6.7×10^{-6}	8.3×10^{-6}	1.6×10^{-5}	10000 km
	2	5.8×10^{-5}	5.9×10^{-5}	1.1×10^{-4}	1.6×10^{-4}	3.9×10^{-4}	5.0×10^{-4}	–	10000 km
	3	1.3×10^{-8}	4.9×10^{-8}	1.8×10^{-7}	2.3×10^{-7}	–	–	–	1000 times
	4*	5.8×10^{-8}	1.4×10^{-7}	5.5×10^{-7}	9.0×10^{-7}	–	–	–	1000 times
	5	4.5×10^{-7}	1.6×10^{-6}	2.1×10^{-6}	1.6×10^{-6}	2.7×10^{-6}	2.2×10^{-5}	–	1000 times
Fault case	6	1.4×10^{-5}	1.8×10^{-5}	2.1×10^{-5}	3.6×10^{-5}	3.8×10^{-5}	4.2×10^{-5}	–	10000 km
	7	2.4×10^{-6}	7.2×10^{-6}	8.1×10^{-6}	8.9×10^{-6}	9.1×10^{-6}	9.6×10^{-6}	–	10000 km
	8	3.1×10^{-7}	5.2×10^{-6}	8.5×10^{-6}	5.5×10^{-6}	–	–	–	10000 km
	9	6.3×10^{-7}	3.0×10^{-6}	2.7×10^{-5}	6.9×10^{-5}	–	–	–	10000 km

* In case 4, the corresponding speeds for speed levels V1–V4 are 20, 30, 40, and 50 km/h, respectively

Table 3 List of damage under tread-after-wear cases

Trial	Case	Damage							Remark
		V1 (100 km/h)	V2 (150 km/h)	V3 (200 km/h)	V4 (250 km/h)	V5 (300 km/h)	V6 (350 km/h)	V7 (400 km/h)	
Normal case	1	4.4×10^{-6}	1.5×10^{-5}	1.9×10^{-5}	1.5×10^{-5}	1.6×10^{-5}	2.3×10^{-5}	4.3×10^{-5}	10000 km
	2	1.2×10^{-4}	1.5×10^{-4}	2.7×10^{-4}	2.9×10^{-4}	4.4×10^{-4}	4.5×10^{-4}	–	10000 km
	3	8.3×10^{-8}	1.0×10^{-7}	4.4×10^{-7}	5.1×10^{-7}	–	–	–	1000 times
	4*	8.6×10^{-8}	1.2×10^{-7}	9.3×10^{-7}	1.2×10^{-6}	–	–	–	1000 times
	5	5.6×10^{-7}	2.0×10^{-6}	3.1×10^{-6}	2.7×10^{-6}	3.4×10^{-6}	3.0×10^{-5}	–	1000 times
Fault case	6	1.7×10^{-5}	2.7×10^{-5}	3.5×10^{-5}	3.9×10^{-5}	4.2×10^{-5}	5.6×10^{-5}	–	10000 km
	7	6.8×10^{-6}	8.8×10^{-6}	9.8×10^{-6}	1.8×10^{-5}	2.1×10^{-5}	2.8×10^{-5}	–	10000 km
	8	4.0×10^{-6}	1.5×10^{-5}	2.4×10^{-5}	2.7×10^{-5}	–	–	–	10000 km
	9	6.5×10^{-7}	5.9×10^{-6}	2.5×10^{-5}	9.0×10^{-5}	–	–	–	10000 km

* In case 4, the corresponding speeds for speed levels V1–V4 are 20, 30, 40, and 50 km/h, respectively

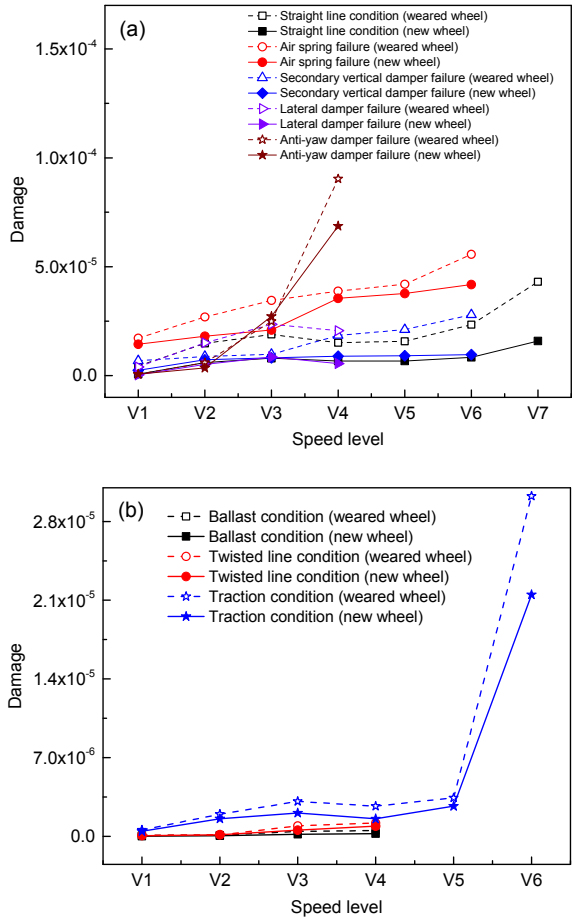

Fig. 10 Damage values per 10 000 km (a) and per 1000 times (b) in different cases

Fig. 10b shows the damage values per 1000 times at various speed levels under the ballast, twisted line, and traction conditions. It can be seen from the figure that, as the speed increases, the damage value becomes larger and larger; damage through the twisted line is larger than that through the ballast; the damage value of the EMU running at 350 km/h (V6) is far greater than when it runs at 300 km/h (V5). The EMU's speed increasing to 350 km/h also requires a systematic evaluation of the vehicle's life.

6 Preparation of the vehicle fatigue load spectrum

In order to more accurately study the fatigue test of the vehicle body, the accuracy of the load spectrum is particularly important. The current vehicle body-related fatigue test is mainly based on the recommendations of EN12663 and the body fatigue test of the AAR truck standard (AAR, 1999). It is extremely urgent to formulate a load spectrum suitable for train body fatigue tests in China. Due to the general characteristics of the railway load spectrum, the load is large and the frequency is high. It is impossible to directly apply the simulated load-time history to the vehicle body through the hydraulic actuator as in an automobile body test. This account compiles the vehicle body fatigue test block spectrum according to the time history of the vehicle body load through simulation and permits the maximum simulation of the actual damage of the car body.

6.1 Data processing of the load-time history of a car body

The data of the load-time history measured on the line is subject to much interference and needs further processing to be converted into an effective load spectrum. The processing of data mainly includes: zero drift processing, abnormal signal processing, filtering processing, and omission of invalid amplitudes. The load spectrum obtained by the dynamic simulation is better, so it is only necessary to omit the invalid amplitude.

In order to accelerate the fatigue test of the vehicle body, such an amplitude should be removed under normal circumstances. The removal of the invalid amplitude should ensure that the damage is basically equivalent to the original signal. Under normal circumstances, it is considered that when the stress-strain curve forms a closed curve, damage will occur. In the S-N curve, when the amplitude of the stress is larger than that of the inflection point, damage will occur, and the signal that does not cause damage will be regarded as the invalid amplitude. However, the invalid amplitude signal determined by the S-N method accounts for more than 90% of the total signal, and then other methods are needed to remove the invalid amplitude. In this case, there are generally two ways: (1) take the maximum amplitude of 5% to 15%, or 5% to 10% as is generally used in the rail vehicle industry; (2) take 50% of the material fatigue limit. In this study we have taken 5% of the maximum amplitude in the load spectrum processing described.

6.2 Extrapolation of the vehicle fatigue load spectrum

The load-time history obtained through dynamic simulation or line measurement is much less than the entire service life of the train. The most important study for a fatigue test is to obtain the change of load time in the whole service life cycle, in order to compare the short load-time history extrapolated to the load-time history throughout the life cycle. This is called the extrapolation of the load spectrum. The extrapolation method of the commonly used load spectrum is shown in Fig. 11. In this paper, the rain flow matrix extrapolation method is used to extrapolate the vehicle fatigue load spectrum.

Assuming that the load-time history of the train running x km is obtained, the total vehicle life is assumed to be y km. Therefore, it is necessary to extrapolate it to the rain flow cycle matrix $\boldsymbol{F}_y$ of y km according to the shape of the rain flow cycle matrix. First, there must be an understanding of the shape of the matrix and then it can be extrapolated to the limit of the rain flow cycle matrix $\boldsymbol{G}$. If this process is discretized into n equal parts, the rain flow matrix $\boldsymbol{G}$ is defined as

$$\boldsymbol{G}=\left(g_{ij}\right)_{i,j=1}^{n},\quad g_{ij}=\lim_{z\to\infty}\frac{E[f_{ij}]}{z}. \tag{7}$$

Assuming that the limit of Eq. (7) is present, the unit f_{ij} in the equation $\boldsymbol{F}_z$ is the number of rain flow cycles. Within the distance of z km, the minimum level is i and the maximum level is j.

In the general line test, only the spectral characteristics of the data are usually given, but the probability of the rain flow cycle is not clearly stated.

Consider a zero mean Gaussian distribution $X(t)$ with $V[X(t)]=1$, $V[X'(t)]=1$. The penetration probability is defined as

$$\mu(u)=\frac{1}{2\pi}\exp\left(-u^2/2\right), \tag{8}$$

and the probability of accumulating rain flow cycles can be expressed as

$$\begin{aligned}\mu_{\mathrm{app}}^{\mathrm{rfc}}(u,v)&=\frac{\mu(u)\mu(v)}{\mu(u)+\mu(v)}\\&=\frac{1}{2\pi\left[\exp(u^2/2)+\exp(v^2/2)\right]},\end{aligned} \tag{9}$$

where u and v indicate a low level and a high level in lever crossing, respectively.

Differentiating u and v gives the probability of the rain flow cycle as

$$\begin{aligned}\lambda_{\mathrm{app}}^{\mathrm{rfc}}(u,v)&=-\frac{\partial^2}{\partial u\partial v}\mu_{\mathrm{app}}^{\mathrm{rfc}}(u,v)\\&=-\frac{uv\cdot\exp\left[(u^2+v^2)/2\right]}{\pi\left[\exp(u^2/2)+\exp(v^2/2)\right]^3}.\end{aligned} \tag{10}$$

The relationship between the cumulative number of rain flow cycles $\boldsymbol{\mu}^{\mathrm{rfc}}$ and the rain flow matrix $\boldsymbol{G}^{\mathrm{rfc}}$ can be expressed as

$$\boldsymbol{G}^{\mathrm{rfc}}=\left(g_{ij}^{\mathrm{rfc}}\right)_{i,j=1}^{n}, \tag{11}$$

$$g_{ij}^{\mathrm{rfc}}=\mu_{i+1,j+1}^{\mathrm{rfc}}-\mu_{i,j-1}^{\mathrm{rfc}}-\mu_{i+1,j}^{\mathrm{rfc}}+\mu_{i,j}^{\mathrm{rfc}}, \tag{12}$$

$$\boldsymbol{\mu}^{\mathrm{rfc}}=\left(\mu_{i,j}^{\mathrm{rfc}}\right)_{i,j=1}^{n}. \tag{13}$$

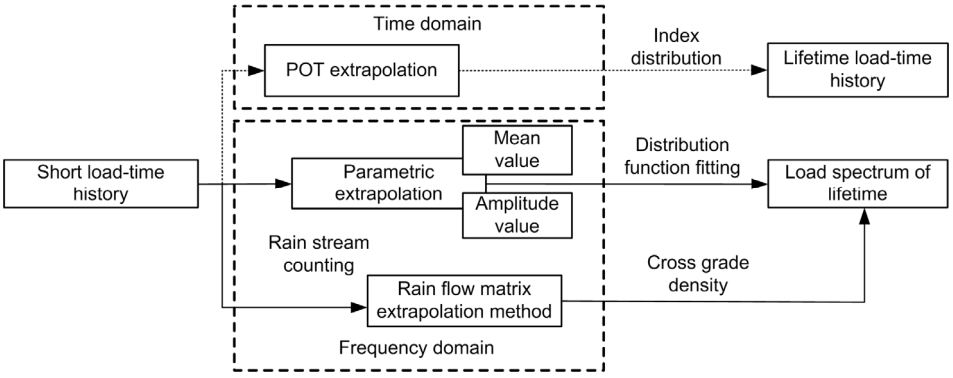

Fig. 11 Method of load spectrum extrapolation (POT indicates peak-over-threshold)

The large load cycle of the vehicle body at its full life is the most important part of the fatigue life prediction, and has a great influence on the damage of the material. The rain flow matrix extrapolation method is not simply extrapolating its frequency, but it is more accurate in predicting the larger load that does not appear in the shorter load-time history according to the extreme value theory. After extrapolation, the amplitude of the load spectrum and the number of cycles are both increased, which is a good indication of the variability of the load under complex conditions.

6.3 Determination of the extreme value of the vehicle fatigue load spectrum

In the fatigue-life prediction of the rail vehicle structure, the data obtained through the line test or simulation is a finite-length load-time history, which cannot truly reflect the maximum stress value that occurs during the entire life of the vehicle body, and can be externally pushed through various extrapolation methods. It is extended to the specified number of load actions, but the determination of the maximum value needs to be determined according to its mathematical statistical distribution form. Many studies have shown that the random load amplitude stress frequency histogram obeys the Weibull distribution, and the load mean obeys a normal distribution. Therefore, the load amplitude and the mean distribution can be statistically calculated according to the Weibull three-parameter distribution and the normal distribution. The parameter fitting and hypothesis testing are performed to obtain the probability density function of the load amplitude and the mean value, and the maximum load spectrum is then estimated.

6.4 Preparation of the vehicle fatigue load spectrum

The process of simplifying the load-time history from the actual measurement or simulation to the load spectrum is called "profiling". In the process of profiling, the following conditions must be met:

1. The fatigue load spectrum compiled should be able to realistically simulate the cyclic load that the vehicle body is subjected to during actual operation so as to enable the fatigue test and estimation of the fatigue life.

2. The variation law of the type of vehicle body load can be predicted based on a limited number of actual measurements or simulation data to obtain a representative load spectrum.

3. The time history of the load obtained by repeated sampling for the same working conditions is not the same, there is a certain degree of dispersion, and the degree of the load spectrum needs to be determined according to the actual situation.

4. Due to the different working conditions of the vehicle body working environment of various railway vehicles, the preparation of the load spectrum must be targeted.

In this study, in order to prepare the fatigue test load spectrum of the car body in a more standard way, the standard load block spectrum is selected. The standard stress block spectrum is used to describe the shape of a typical stress block spectrum. There are two main types of standard stress block spectrum, one with a binomial frequency distribution and the other with an exponential (straight line) probability distribution, as shown in Fig. 12. It can be seen from the figure that the block spectrum changes with the spectrum parameter p, and the parameter p corresponds to the damage potential of the component:

$$v_\sigma = \sqrt[k_\sigma]{\sum_{i=1}^{j} \frac{h_i}{H}\left(\frac{\sigma_{ai}}{\sigma_{a1}}\right)^{k_\sigma}}, \tag{14}$$

where v_σ represents the damage potential factor of the component or material, i represents the load step, j represents the total number of load steps, h_i represents the number of cycles of the ith load step, H represents the total number of load cycles, σ_{ai} represents the stress amplitude of the load step, σ_{a1} represents the stress amplitude of the first load step, and k_σ represents the slope of the member S-N curve at 10^6 cycles.

The standard load block spectrum of the car body bolster is finally shown in Table 4.

6.5 Implementation of the vehicle body fatigue test

The constructed vehicle fatigue test bench has a basin-like structure, and two sets of six-DOF (degree of freedom) platforms are placed inside. The longitudinal tie rods with closed ring beams are fixed with large-diameter screws, and the screw rods are fixed by

the screw support of the Havel structure. On the T-slot platform, the loading beam includes a fixed-end reaction-force beam, a moving-end reaction-force beam, and a moving load beam. A fixed-end reaction-force beam is fixed to the left end of the longitudinal tie rod, locked with a locking round nut, and loaded with a hydraulic servo actuator. The actuator is mounted on the fixed-end reaction-force beam to apply force to the position of the coupler. Fig. 13 is a cross-sectional view showing the structure of a vehicle body fatigue test stand. Fig. 14 shows the fatigue test of the standard load block spectrum of Table 4 on the fatigue test bench.

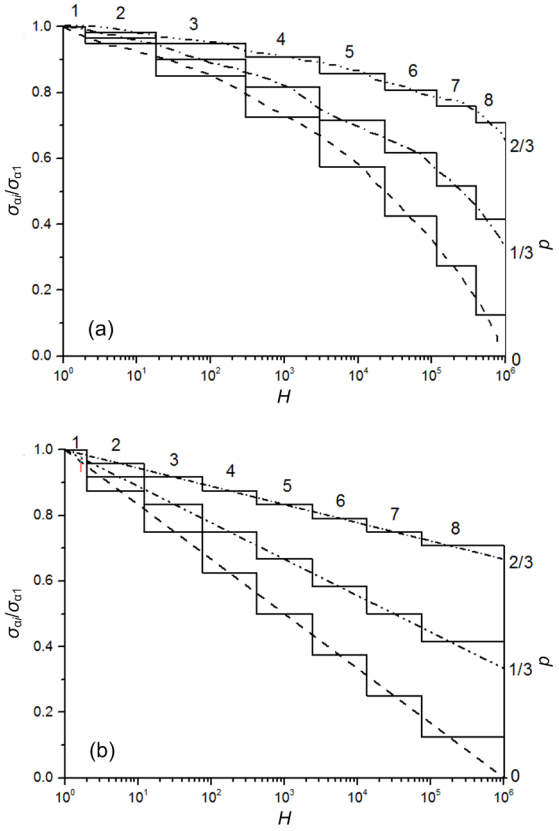

Fig. 12 Binomial (a) and exponential (b) distributions of standard stress block spectra

Table 4 Standard load block spectrum of car body beam

a_x	a_y	a_z	h_i	H
0.13	0.19	0.22	2	2
0.10	0.14	0.20	16	18
0.08	0.10	0.19	280	298
0.05	0.07	0.15	2720	3018
0.04	0.05	0.11	20 000	23 018
0.03	0.04	0.08	92 000	115 018
0.02	0.03	0.06	280 000	395 018
0.01	0.01	0.02	604 982	1 000 000

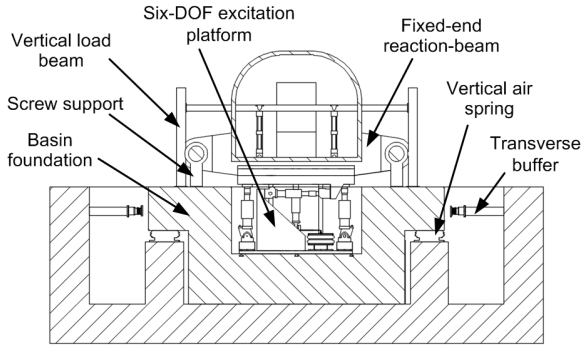

Fig. 13 Cross-sectional view of car body fatigue test bench

Fig. 14 Car body of the EMU on the fatigue test bench

7 Conclusions

1. Through dynamic simulation, the load spectrum obtained at different speed levels under different line conditions, different fault conditions, and different tread conditions in the same working condition is analyzed. It is found that the accelerations of the three directions of the vehicle body increase with the increase of speed. When the train passes a curve, it will cause the lateral acceleration to be larger. The passage of a turnout or twisted line will cause the acceleration of the car body to increase in three directions. With an empty spring failure, the vertical acceleration of the car body will increase significantly. Failure of the anti-yaw damper will cause a significant increase in the lateral acceleration of the car body and failure of the secondary lateral and vertical dampers will cause an increase in accelerations in three directions, but the increase is not obvious. The accelerations of the car body increase for wear-type

tread under different conditions and speed levels relative to the original tread.

2. The power spectral density function analysis of the vehicle body acceleration load-time history shows that the vibration energy of the vehicle body is concentrated below 20 Hz under various conditions. The structural fatigue life prediction analysis is carried out by using the vehicle body acceleration load-time history, and the damage values under various working conditions are obtained. The results show that vehicle body damage increases with increased speed and the wear type tread exhibits that more than the non-wearing type. Considering significant damage to the car body, it is found that, under fault conditions, when the speed is low (v<200 km/h), the failure of the air spring causes significant damage to the car body but other conditions are not harmful to it; when the speed is v>200 km/h, the failure of the anti-yaw damper causes the greatest damage to the car body. When the train passes through a turnout or twisted line, it will also cause certain damage to the car body but, because the speed is lower when passing through these areas, the impact is not very large. When the train is subjected to traction braking, the damage increases as the speed increases. When the traction speed reaches 300 km/h or more, the damage increases sharply.

3. We introduce the vehicle body load spectrum processing method, and finally take 5% of the maximum value of the load as the invalid amplitude. The parameters are fitted according to the distribution shape of the mean value and the amplitude value, and the extreme value is determined. A standard 8-level load spectrum suitable for the vehicle body fatigue test was prepared, and the vehicle body was subjected to a fatigue test of 10 million times (it is repeated 10 times to the standard load block spectrum) on the vehicle body fatigue test bench.

Contributors

Huan-yun DAI designed the research. Lu JIA and Ye SONG processed the corresponding data. Lu JIA wrote the first draft of the manuscript. Huan-yun DAI and Ye SONG helped to organize the manuscript. Lu JIA and Ye SONG revised and edited the final version.

Conflict of interest

Lu JIA, Huan-yun DAI, and Ye SONG declare that they have no conflict of interest.

References

AAR (Association of American Railroad), 1999. Locomotive and Rolling Stock Standard Manual. AAR, Washington, USA.

BSI (British Standards Institution), 2014. Guide to Fatigue Design and Assessment of Steel Products, BS 7608:2014. BSI, London, UK.

Gongjiang MS, 2003. The strength of carbody for Shinkansen cars and safety evaluation. *Foreign Rolling Stock*, 40(6): 12-16 (in Chinese). https://doi.org/10.3969/j.issn.1002-7610.2003.06.004

Gou G, Zhang M, Chen H, et al., 2015. Effect of humidity on porosity, microstructure, and fatigue strength of A7N01S-T5 aluminum alloy welded joints in high-speed trains. *Materials & Design*, 85:309-317. https://doi.org/10.1016/j.matdes.2015.06.177

Gutiérrez-Carvajal RE, Betancur GR, Barbosa J, et al., 2018. Full scale fatigue test performed to the bolster beam of a railway vehicle. *International Journal on Interactive Design and Manufacturing (IJIDeM)*, 12(1):253-261. https://doi.org/10.1007/s12008-016-0361-0

Hou B, 2016. The Load Spectrum Study on High-speed EMU Body. MS Thesis, Southwest Jiaotong University, Chengdu, China (in Chinese).

IIW (International Institute of Welding), 2016. Recommendations for Fatigue Design of Welded Joints and Components, IIW-2259-15:2016. IIW, Wilhelmshaven, Germany.

Ju YZ, 2013. High-speed EMU Aluminum Alloy Weld Fatigue Life Prediction of Vehicle. MS Thesis, Dalian Jiaotong University, Dalian, China (in Chinese).

Jun HK, Jung HS, Lee DH, et al., 2010. Fatigue crack evaluation on the underframe of EMU carbody. *Procedia Engineering*, 2(1):893-900. https://doi.org/10.1016/j.proeng.2010.03.096

Li FS, 2018. Research on Vibration and Fatigue of Carbody for EMU under Service Environment. PhD Thesis, Southwest Jiaotong University, Chengdu, China (in Chinese).

Li XF, 2008. Predicting Fatigue Life of Rail Vehicle Welded Structure Based on Virtual Fatigue Test. PhD Thesis, Dalian Jiaotong University, Dalian, China (in Chinese).

Liu K, 2013. The Research of Ability of Anti-fatigue for Aluminum Alloy Car Body. MS Thesis, Dalian Jiaotong University, Dalian, China (in Chinese).

Liu YB, 2015. Analysis on Ground Effects of High-speed Trains and the Resultant Fatigue Damage to the Equipment Bay. PhD Thesis, Beijing Jiaotong University, Beijing, China (in Chinese).

Lu X, 2010. Vibration Fatigue Life Analysis on Rigid-flexible Coupling of CRH3 Car Body. MS Thesis, Dalian Jiaotong University, Dalian, China (in Chinese).

Lu YH, Dang LY, Zhang X, et al., 2018a. Analysis of the dynamic response and fatigue reliability of a full-scale carbody of a high-speed train. *Proceedings of the Institution of Mechanical Engineers, Part F: Journal of Rail and Rapid Transit*, 232(7):2006-2023.

https://doi.org/10.1177/0954409718757295

Lu YH, Zheng HY, Lu C, et al., 2018b. Analysis methods of the dynamic structural stress in a full-scale welded carbody for high-speed trains. *Advances in Mechanical Engineering*, 10(10):1-16. https://doi.org/10.1177/1687814018805917

Miao BR, Zhang LM, Zhang WH, et al., 2010. High-speed train carbody structure fatigue simulation based on dynamic characteristics of the overall vehicle. *Journal of the China Railway Society*, 32(6):101-108 (in Chinese). https://doi.org/10.3969/j.issn.1001-8360.2010.06.017

Oomura K, Okuno S, Kawai S, et al., 1992. Fatigue test of an actual car body structure (1st report, the testing method and its accuracy). *Transactions of the Japan Society of Mechanical Engineers Series A*, 58(545):20-25 (in Japanese).

Qin HF, 2017. Study on the Load Spectrum of Chinese Standard EMUs. MS Thesis, Beijing Jiaotong University, Beijing, China (in Chinese).

Song Y, Wu PB, Jia L, 2016. Study of the fatigue testing of a car body underframe for a high-speed train. *Proceedings of the Institution of Mechanical Engineers, Part F: Journal of Rail and Rapid Transit*, 230(6):1614-1625. https://doi.org/10.1177/0954409715618425

Wang YW, 2015. The Corbel Fatigue Strength of CRH-2 EMU Based on the Measured Load. MS Thesis, Beijing Jiaotong University, Beijing, China (in Chinese).

Wang ZY, 2016. The Study on the Vibration Fatigue of Mono-car Body Made of Aluminum Alloy. MS Thesis, Southwest Jiaotong University, Chengdu, China (in Chinese).

Wei QS, 2018. Study on Fatigue Crack Propagation of the Al Alloy Crossbeam in High Speed EMU Car Body. MS Thesis, Beijing Jiaotong University, Beijing, China (in Chinese).

Xie JL, Zhang Y, Xie YY, 2010. Dynamic response and fatigue strength of depressed center flat frame. *Journal of Mechanical Engineering*, 46(16):16-22 (in Chinese). https://doi.org/10.3901/JME.2010.16.016

Xue GJ, 2013. Inference and Calibration of Rail Vehicles Load Spectrum Based on Mathematical Statistics Methods. MS Thesis, Beijing Jiaotong University, Beijing, China (in Chinese).

Yan X, 2009. The Compile of Longitudinal Load Spectrum for Da-Qin Line 20,000-ton Heavy-load Train. MS Thesis, Beijing Jiaotong University, Beijing, China (in Chinese).

Yan XD, 2014. Reliability Study of High Speed Train Equipment Bay Bottom Plates. MS Thesis, Beijing Jiaotong University, Beijing, China (in Chinese).

Yang GW, 2005. Simulation of Prediction of Fatigue Life for Component of Railway Vehicle. PhD Thesis, Southwest Jiaotong University, Chengdu, China (in Chinese).

Yang YB, Liang XJ, Hung HH, et al., 2017. Comparative study of 2D and 2.5D responses of long underground tunnels to moving train loads. *Soil Dynamics and Earthquake Engineering*, 97:86-100. https://doi.org/10.1016/j.soildyn.2017.02.005

Zhang SG, 2008. Study on testing and establishment method for the load spectrum of bogie frame for high-speed trains. *Science in China Series E: Technological Sciences*, 51(12):2142-2151. https://doi.org/10.1007/s11431-009-0025-4

Zhang SX, 2016. Load Spectrum Compiling and Life Prediction Simulation of High Speed Train Car Body Based on the Acceleration Life Test. MS Thesis, Southwest Jiaotong University, Chengdu, China (in Chinese).

中文概要

题　目：基于动力学仿真载荷谱的车体疲劳损伤评估及试验技术研究

目　的：基于动力学仿真载荷谱对动车组车体进行疲劳损伤评估，并在试验台上进行验证。

创新点：1. 基于动力学仿真得到车体服役载荷谱；2. 通过损伤评估得到车体在各种工况下的疲劳损伤，并在试验台上将载荷谱应用于整车车体。

方　法：1. 通过动力学仿真，对同一工况不同速度等级、不同线路条件、不同故障工况和不同踏面情况下得到的载荷谱进行分析。2. 利用车体的加速度载荷时间历程对其进行结构疲劳寿命预测分析，得到各个工况下的损伤值。

结　论：1. 随着速度的提高，车体三个方向的加速度越来越大；列车通过曲线时，横向加速度均值偏大；道岔通过和扭曲线路都会引起车体三个方向加速度的增加；空簧失效条件下，车体垂向加速度明显增大；抗蛇行减振器失效会引起车体横向加速度的明显增加；二系横向和垂向减振器的失效会引起三个方向的加速度增大，但是不明显；在各个工况及速度级条件下，相对于原始踏面，车体在磨耗型踏面的加速度更大。2. 对所得车体加速度载荷时间历程进行功率谱密度函数分析发现，各种条件下的车体振动能量主要集中在 20 Hz 以下。3. 随着速度的增加，车体损伤增加；磨耗型踏面比非磨耗型踏面对车体损伤大；故障工况下，当速度小于 200 km/h 时，只有空簧失效对车体损伤较大；当速度大于 200 km/h 时，抗蛇行减振器失效对车体产生的损伤最大；道岔和扭曲线路会对车体产生一定的损伤，但影响不大；当列车进行牵引制动时，随着速度的提高，损伤也相应增加，并且当牵引速度大于 300 km/h 时，损伤会急剧增加。

关键词：动力学建模；车体；载荷时间历程；疲劳；损伤